ACS Catalysis

Research Article

pubs.acs.org/acscatalysis

DFT Study on Mechanism of N-Alkylation of Amino Derivatives with Primary Alcohols Catalyzed by Copper(II) Acetate

Guo-ming Zhao,[†,‡] Hui-ling Liu,*[,†] Dan-dan Zhang,[†] Xu-ri Huang,*[,†] and Xue Yang[‡]

[†]State Key Laboratory of Theoretical and Computational Chemistry, Institute of Theoretical Chemistry, Jilin University, Changchun, 130023, China

[‡]College of Science, Jilin Institute of Chemical Technology, Jilin, 132022, China

Supporting Information

ABSTRACT: DFT calculations have been carried out to study the mechanism of $Cu(AcO)_2$-catalyzed N-alkylation of amino derivatives with primary alcohols. The calculations indicate that tBuOK is necessary for the generation of the active catalyst from $Cu(AcO)_2$ and that the catalytic cycle involves three sequential steps: (1) Cu-catalyzed alcohol oxidation to give the corresponding aldehyde and copper hydride, (2) aldehyde-amine condensation to generate an imine, (3) imine reduction to yield the expected N-alkylation secondary amine product and to regenerate the active catalyst. Based on the comparison of different reaction pathways, we conclude that the outer-sphere hydrogen transfer in a stepwise manner is the most favorable pathway for both alcohol oxidation and imine reduction. Thermodynamically, alcohol oxidation and imine formation are all uphill, but imine reduction is downhill significantly, which is the driving force for the catalytic transformation. Using the energetic span model, we find that the turnover frequency-determining transition state (TDTS) and the turnover frequency-determining intermediate (TDI) are the hydride transfer transition state for imine reduction and the active catalyst, respectively. The calculated turnover frequency (TOF) roughly agrees with the experimental observation and, therefore, further supports the validity of the proposed hydrogen transfer mechanism.

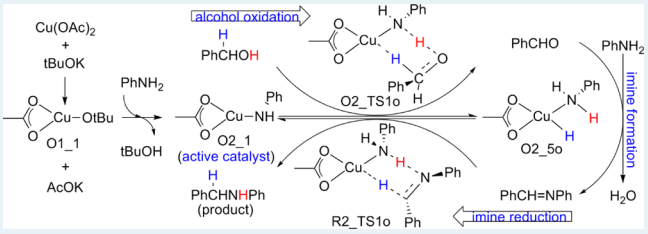

KEYWORDS: *DFT calculations, primary alcohols, amino derivatives, N-alkylation reaction, $Cu(AcO)_2$, tBuOK, hydrogen transfer mechanism*

INTRODUCTION

Formation of the carbon−nitrogen (C−N) bond is an active area of research for organic synthesis because nitrogen-containing compounds are necessary in building blocks for robust pharmacophores and useful bioactive compounds.[1] Traditionally, C−N bonds are formed via substitution with alkyl/aryl halides[2] or reductive amination from carbonyl compounds.[3] These methods are efficient but may suffer from the generation of too much waste. Environmental concerns in chemistry have increased the demand for environmentally friendly methods, which leads to the development of new C−N bond-forming methods. Recently, significant attention has been paid to transition metal-catalyzed N-alkylation of amino derivatives with primary alcohols via a hydrogen transfer (or hydrogen-borrowing) process.[4] This method is apparently attractive, not only because alcohols are nontoxic, inexpensive, and readily available but also because monoalkylated products with high selectivity can be obtained and the only byproduct is water. Experimentally, Ru,[5] Pt,[6] Rh,[7] and Ir[8] catalysts have been employed for this hydrogen transfer process. However, a simple, selective, and economical catalyst is necessary for the future profit-driven synthesis. In this regard, $Cu(OAc)_2$ is a good option.

$Cu(OAc)_2$-catalyzed N-alkylation of sulfonamides with alcohols was first demonstrated in 2009.[9] Subsequently, a mechanistic study was also presented using sulfonamides as a nucleophile in the air.[10] However, these two papers have only considered N-alkylation of sulfonamides with alcohols, while other amino derivatives, such as aromatic and heteroaromatic amines as well as phosphinamides, carboxamides, and phosphazenes, are not referred to. In 2010, another protocol about $Cu(OAc)_2$-catalyzed N-alkylation of various amino derivatives with primary alcohols appeared (eq 1).[11] The mechanistic considerations indicated that

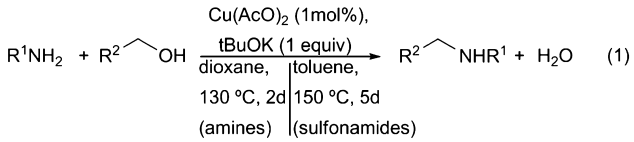

R^1=Ph, 4-MeOC_6H_4, 2-MeOC_6H_4, 3-ClC_6H_4, 2-Pyridyl, 2-Pyrimidyl, $MeSO_2$, 4-Me$C_6H_4SO_2$, 4-Me$OC_6H_4SO_2$; R^2=Ph, 4-MeOC_6H_4, 4-ClC_6H_4, 4-MeC_6H_4, 2-MeOC_6H_4, 3-ClC_6H_4, 1-$C_{10}H_7$, 2,3-$(OCH_2O)C_6H_3$, $(CH_2)_5CH$.

the N-alkylation reaction would proceed via the known hydrogen transfer process in the presence of base and that the catalytic process involved three sequential steps: (1) alcohol oxidation to

Received: April 9, 2014
Revised: May 25, 2014
Published: May 27, 2014

   dx.doi.org/10.1021/cs5004678 | ACS Catal. 2014, 4, 2231−2240

give the corresponding aldehyde and Cu hydride species, (2) aldehyde-amine condensation to generate imine and water, and (3) imine reduction to yield the expected N-alkylation secondary amine product and to regenerate the catalyst.[12] Theoretically, two key transformations of the N-alkylation reaction, alcohol oxidation and imine reduction, have been studied extensively, but mainly with Ru and Ir complexes.[13] So far as we know, there has been no theoretical study on Cu(II)-catalyzed N-alkylation of amino derivatives with alcohols. With this paper, we wish to fill the lack of information. The objectives of the present investigation are as follows: (1) to clarify the role of the base, (2) to find the active catalyst, (3) to identify the most favorable reaction pathway, (4) to locate the rate-determining key states.

COMPUTATIONAL DETAILS

Molecular geometries of all complexes were fully optimized with the tight convergence criteria (SCF = tight) at the B3LYP[14,15](SMD—Truhlar and co-workers'solvation model which does an IEFPCM calculation with radii and nonelectrostatic terms,[16] 1,4-dioxane)/BSI level (BSI designated the basis set combination of LanL2DZ[17,18] for Cu and 6-31G (d,p)[19] for all nonmetal atoms). The reason why we chose DFT method B3LYP was that this method has been shown to be a good method for studying Cu-catalyzed organic reactions.[20] Frequency calculations at the same level of theory were also conducted to identify the stationary point as a minimum (zero imaginary frequency) or transition state (one imaginary frequency) and to provide thermal correction to Gibbs free energy at 403.15 K. Intrinsic reaction coordinate (IRC)[21] calculations were carried out to confirm the transition state connecting the correct reactant and product on the potential energy surface. Single-point energy calculations were performed on the stationary points at the M06[22](SMD, 1,4-dioxane)/BSII level (BSII denoted the basis set combination of LANL2TZ(f)[18,23] for Cu and 6-311++G(2df,2p) for all nonmetal atoms). The M06 functional was chosen because it could describe noncovalent interactions and apply in organometallic chemistry. Single-point energies corrected by Gibbs free energy corrections were used in the following discussion, unless otherwise specified. We also performed M06//BLYP,[15,24] M06//TPSSTPSS,[25] and M06//M06 DFT calculations to verify the conclusions drawn from M06//B3LYP results. The basis sets, the solvent model, and the convergence criteria for those DFT calculations were the same as used in the M06//B3LYP calculations. All calculations were carried out by using Gaussian 09 programs.[26]

RESULTS AND DISCUSSION

Model Reaction. As shown in eq 1, $Cu(AcO)_2$ and tBuOK are used as the catalyst precursor and the base, respectively. In the following calculations, temperature = 403.15 K, solvent = 1,4-dioxane, and N-alkylation of aniline ($PhNH_2$) with benzyl alcohol ($PhCH_2OH$) is chosen as the model reaction.

Alcohol Oxidation. *Equilibrium between Different Copper Complexes.* At the beginning of the reaction, some Cu(II) complexes may exist in equilibrium through ligand exchange in the solution. As shown in Figure 1A, $Cu(AcO)_2$ can exchange AcO^- with the $tBuO^-$ of tBuOK to form a tricoordinated Cu(II) complex O1_1. This process is exergonic by 9.7 kcal mol^{-1}. Then coordination of $PhNH_2$ to O1_1 leads to the formation of a more stable tetracoordinated intermediate NH_1. The transition state NH_TS1 is 9.1 kcal mol^{-1} higher than NH_1. In this proton transfer transition state, the proton is located between the alcohol and the amine (O···H = 1.206 Å and N···H = 1.300 Å, see Figure 1B), closer to the alcohol. This transition state connects to intermediate NH_2, containing an anionic aniline ligand and a tert-butanol ligand. Complex NH_2 is an unstable intermediate and can easily dissociate its tBuOH ligand to give another tricoordinated Cu(II) complex O2_1. The fact that O2_1 and O1_1 have a vacant coordination site at the metallic center, respectively, makes the two tricoordinated Cu(II) complexes the candidates for the active catalysts in the following calculations.

O2_1- and O1_1-Catalyzed Alcohol Oxidation. With the proposed active catalysts in hand, next we will study all the possible reaction pathways in alcohol oxidation. First, we consider O2_1-catalyzed benzyl alcohol oxidation via the outer-sphere

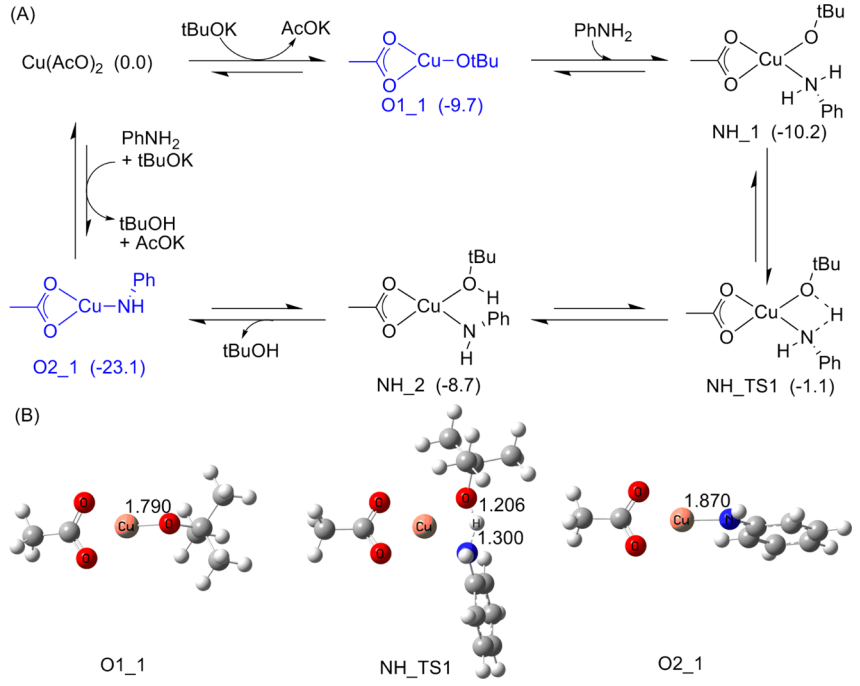

Figure 1. (A) Equilibrium between different Cu(II) complexes. Values in parentheses are Gibbs free energies in kcal mol^{-1}. (B) Optimized structures of O1_1, NH_TS1 (1270i cm^{-1}), and O2_1, together with the key bond lengths in Å.

dx.doi.org/10.1021/cs5004678 | ACS Catal. 2014, 4, 2231−2240

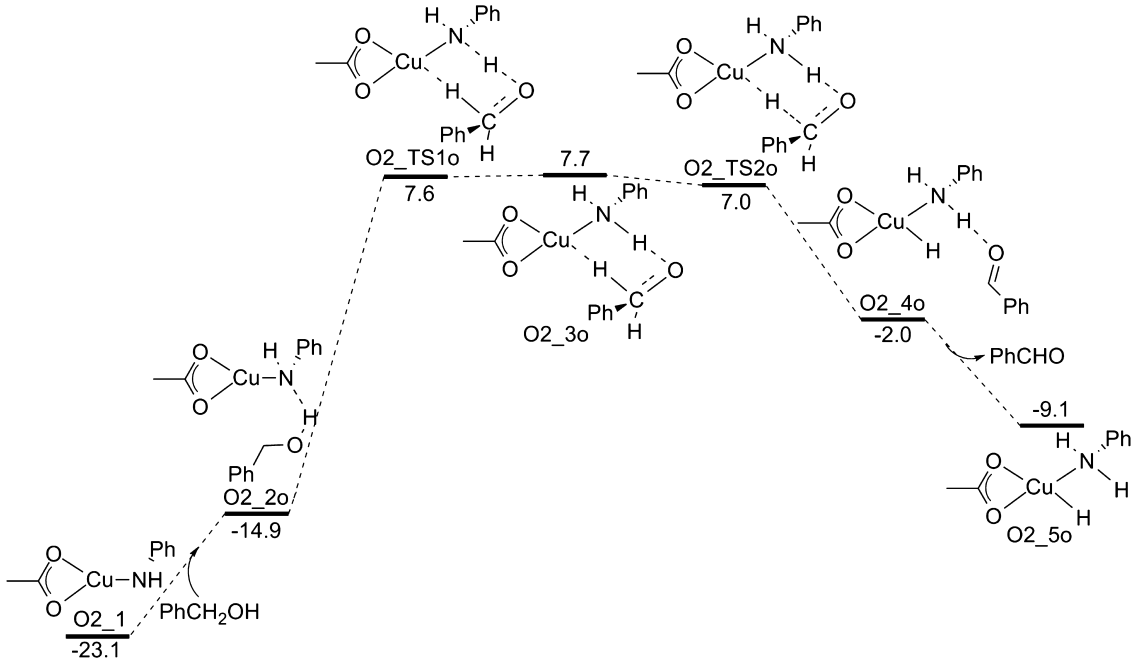

Figure 2. Energy profile for O2_1-catalyzed benzyl alcohol oxidation via the outer-sphere hydrogen transfer pathway. The relative Gibbs free energies are given in kcal mol^{-1}.

hydrogen transfer pathway (this pathway is defined as O2o; note: O, 2, and o denote alcohol oxidation, O2_1, and outer-sphere, respectively). As shown in Figure 2, the initial hydrogen-bonded structure O2_2o is 8.2 kcal mol^{-1} higher than O2_1 + $PhCH_2OH$. This intermediate is well prepared for proton transfer from the alcohol to the amine. The transition state O2_TS1o for the proton transfer has been located at a free energy of 22.5 kcal mol^{-1} above intermediate O2_2o. In this six-membered transition state, the α hydrogen has interactions with the Cu center (C···H = 1.189 Å and Cu···H = 1.881 Å, see Figure 3) and the proton is located between the alcohol and the anionic aniline (O···H = 1.372 Å and N···H = 1.144 Å), closer to the amine. This transition state leads to the formation of intermediate O2_3o, which is stabilized by an intramolecular NH···O hydrogen bond of 1.597 Å and a C−H···Cu interaction characterized by C−H and Cu···H bond distances of 1.212 and 1.826 Å, respectively. It is worthwhile to note that the optimized intermediate O2_3o is higher than the transition state O2_TS1o and O2_TS2o in terms of Gibbs free energy, 30.8 vs 30.7 and 30.1 kcal mol^{-1} relative to O2_1 + $PhCH_2OH$, but lower in terms of electronic energy, 13.9 vs 15.3 and 14.8 kcal mol^{-1}. A similar situation has happened in the nitrogen heterocycles dehydrogenation[27] and the imine hydrogenation.[28] The transition state O2_TS2o for the hydride transfer also has a six-membered structure, which contains a NH···O hydrogen bond of 1.777 Å and a strong C···H···Cu interaction characterized by C···H and Cu···H bond distances of 1.588 and 1.616 Å, respectively. This transition state leads to the H-bonded intermediate O2_4o. Although intermediate O2_4o is 9.0 kcal mol^{-1} in free energy lower than O2_TS2o, the H bond in O2_4o is unstable and easily breaks to release the aniline-coordinated Cu hydride O2_5o and benzaldehyde. This release process is exergonic by 7.1 kcal mol^{-1}. The Cu−H and N−H bond lengths in O2_5o are 1.553 and 1.017 Å, respectively. The geometry of O2_5o with the H−Cu−N−H dihedral angle of 22.756° is very important for future imine reduction because this geometry easily forms a six-membered structure with an imine, which will facilitate the hydride transfer from O2_5o to the imine. Overall, O2_1-catalyzed alcohol oxidation via the outer-sphere hydrogen transfer pathway is endergonic by 14.0 kcal mol^{-1} and occurs with successive steps having accessible energy barriers.

In the case of O2_1 as the catalyst via the inner-sphere hydrogen transfer pathway (defined as O2i; note: O, 2, and i denote alcohol oxidation, O2_1, and inner-sphere, respectively), the beginning tricoordinated Cu(II) species is found to be able to form a tetracoordinated intermediate O2_2i with $PhCH_2OH$ by costing a free energy of 14.1 kcal mol^{-1} (Figure 4). This intermediate is well prepared for proton transfer from the alcohol to the amine. The transition state O2_TS1i for proton transfer is located at a free energy of 8.9 kcal mol^{-1} above O2_2i, in which the proton lies midway between the O of benzyl alcohol and the N of aniline (O···H = 1.194 Å and N···H = 1.312 Å, see Figure 3). This transition state leads to the formation of the aniline-coordinated intermediate O2_3i. However, this tetracoordinated intermediate O2_3i is not well prepared for β-H elimination of its deprotonated benzyl alcohol ligand because no active site is available at the metallic center. The dissociation of aniline from O2_3i leads to a tricoordinated metal alkoxide O2_4i which has an active site on Cu. This dissociation step only requires a free energy of 0.8 kcal mol^{-1}. The transition state O2_TS2i for the β-H elimination is 19.5 kcal mol^{-1} higher than O2_4i, in which the hydride is located between the carbon and the copper (C···H = 1.786 Å and Cu···H = 1.629 Å), closer to the copper. In this four-membered transition state, the Cu···O distance and C−O length are 12% longer and 9% shorter than those in O2_4i, respectively, which confirms the Cu−O bond-breaking and C═O bond-forming processes. This transition state connects to the PhCHO-coordinated Cu hydride O2_5i, which is not a stable Cu hydride although it is 11.3 kcal mol^{-1} lower than O2_TS2i. The release of PhCHO from complex O2_5i gives the Cu hydride O2_6i, which is 2.7 kcal mol^{-1} more stable than O2_5i. However, in the calculations, we find that intermediate O2_6i is not the most stable either. A much more stable Cu

dx.doi.org/10.1021/cs5004678 | ACS Catal. 2014, 4, 2231−2240

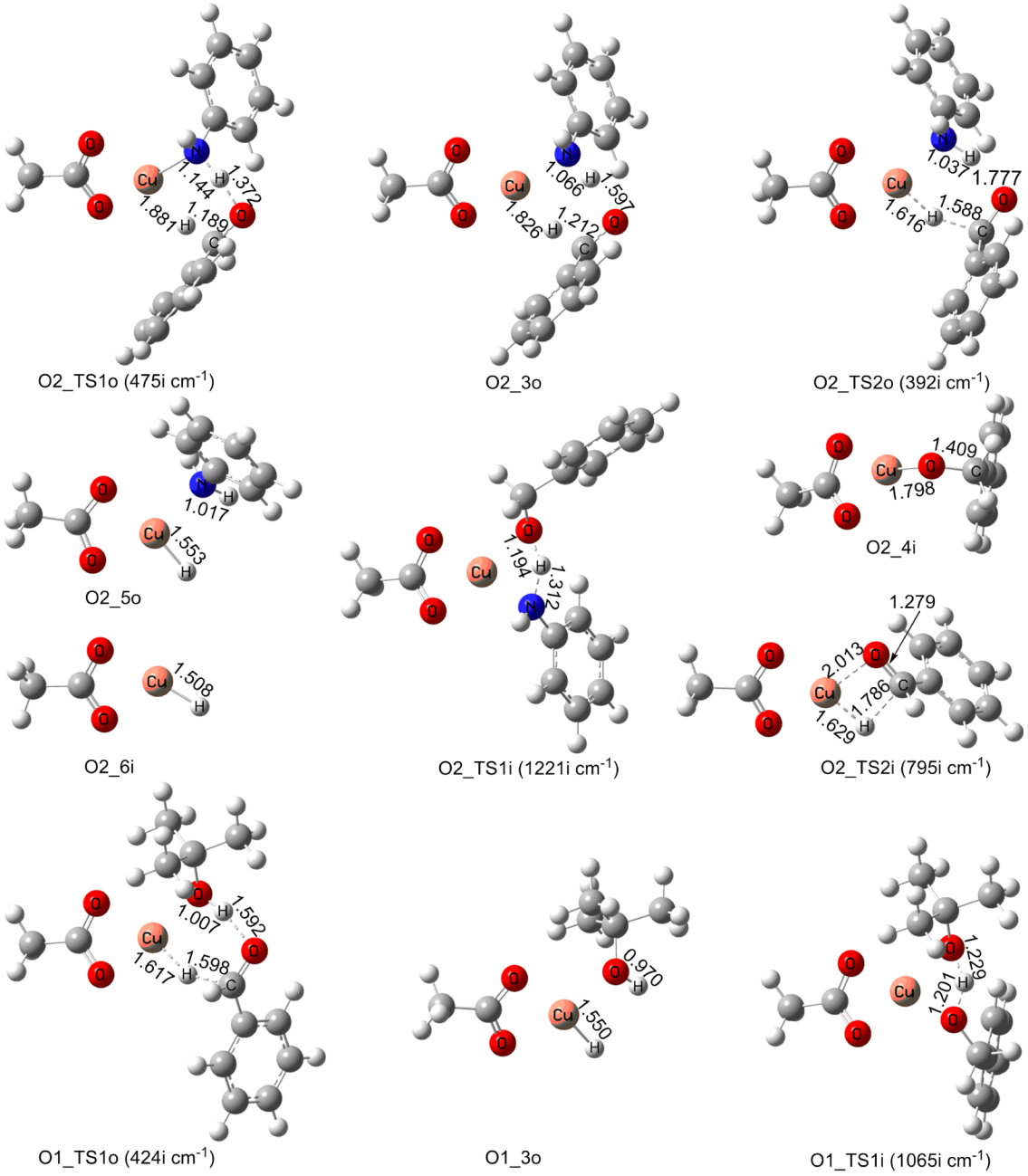

Figure 3. Optimized structures of selected species with selected bond distances (in Å) for benzyl alcohol oxidation. The value in parentheses is the single imaginary frequency that the transition state has.

hydride is the aniline-coordinated Cu complex O2_5o, which can be obtained either by exchanging the PhCHO ligand in O2_5i with $PhNH_2$ or by coordination of $PhNH_2$ to complex O2_6i. The Cu hydride O2_5o is 6.0 kcal mol^{-1} more stable than O2_5i and 3.3 kcal mol^{-1} more stable than O2_6i. Overall, O2_1-catalyzed alcohol oxidation via the inner-sphere hydrogen transfer pathway is endergonic by 14.0 kcal mol^{-1}.

In the case of O1_1 as the catalyst via the outer-sphere hydrogen transfer pathway, the beginning tricoordinated copper-(II) complex O1_1 can form a H-bonded intermediate O1_2o with $PhCH_2OH$ by costing a free energy of 5.7 kcal mol^{-1} (Figure 5). The transition state O1_TS1o for the concerted proton and hydride transfer is located at a free energy of 14.8 kcal mol^{-1} above O1_2o. In this six-membered transition state, the α hydrogen and hydroxy hydrogen of benzyl methanol have interactions with the Cu center and tert-butanol oxygen, respectively. The distances of C···H, Cu···H, $PhCH_2O$···H, and tBuO···H are 1.598, 1.617, 1.592, and 1.007 Å, respectively (Figure 3). This transition state leads to the tBuOH-coordinated Cu hydride O1_3o and PhCHO. In this Cu hydride, the Cu−H and O−H distances are 1.550 and 0.970 Å, respectively. Subsequently, O1_3o exchanges its tBuOH ligand with $PhNH_2$ to give a more stable Cu hydride O2_5o.

In the case of O1_1 as the catalyst via the inner-sphere hydrogen transfer pathway, the beginning tricoordinated copper(II) complex O1_1 can form a tetracoordinated intermediate O1_2i with $PhCH_2OH$ by costing a free energy of 4.0 kcal mol^{-1} (Figure 6). The transition state O1_TS1i for proton transfer of $PhCH_2OH$ has been located at a free energy of 3.3 kcal mol^{-1} above O1_2i, in which the $PhCH_2O$···H and tBuO···H distances

dx.doi.org/10.1021/cs5004678 | ACS Catal. 2014, 4, 2231−2240

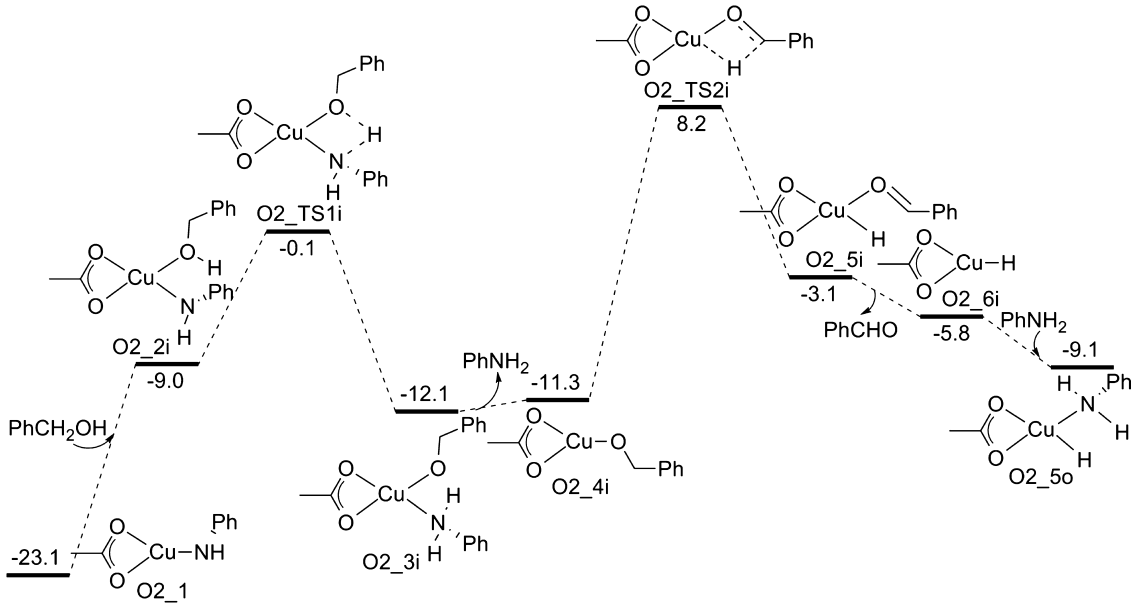

Figure 4. Energy profile for O2_1-catalyzed benzyl alcohol oxidation via the inner-sphere hydrogen transfer pathway. The relative Gibbs free energies are given in kcal mol^{-1}.

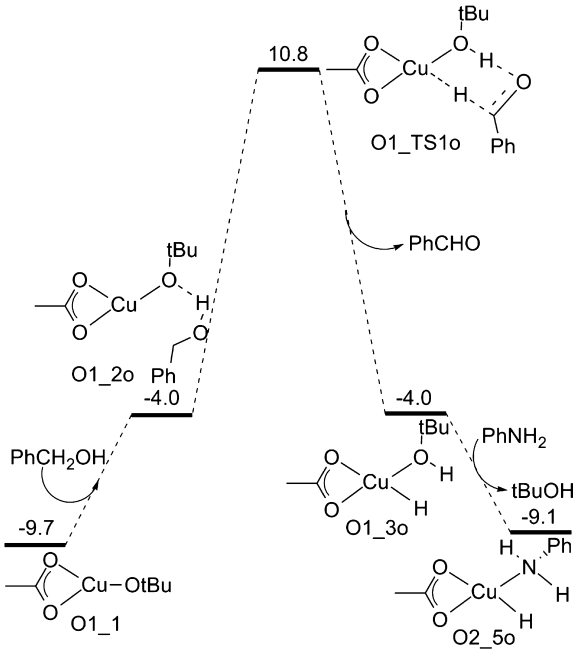

Figure 5. Energy profile for O1_1-catalyzed benzyl alcohol oxidation via the outer-sphere hydrogen transfer pathway. The relative Gibbs free energies are given in kcal mol^{-1}.

are 1.201 and 1.229 Å, respectively (see Figure 3). This transition state O1_TS1i leads to the formation of tetracoordinated intermediate O1_3i, which can easily decompose into the metal alkoxide O2_4i and tBuOH since it is less stable than O2_4i + tBuOH by 1.5 kcal mol^{-1}. The subsequent β-H elimination process is the same as that in O2i, which is not repeated here for brevity's sake.

Comparison of Different Alcohol Oxidation Pathways. The apparent activation energies for O1_1-catalyzed alcohol oxidation in Figures 5 and 6 are 20.5 and 19.5 kcal mol^{-1}, respectively. These two barriers are much higher than the activation energy for the formation of O2_1 (9.1 kcal mol^{-1}, Figure 1A), so that O1_1 has reacted with $PhNH_2$ to generate O2_1 and tBuOH before O1_1 catalyzes benzyl alcohol oxidation to give benzaldehyde via the outer-sphere or inner-sphere hydrogen transfer pathway. This fact means that O1_1 cannot be taken as the starting material for alcohol oxidation when we determine how the activation barrier should be calculated, but it does not mean that O1_1 is not a reactive intermediate.

Treating O2_1 as the starting species, two new alcohol oxidation pathways containing O1_1 can be proposed: one is O2_1 → NH_2 → NH_TS1 → NH_1 → O1_1 → O1_2o → O1_TS1o → O1_3o → O2_5o (defined as O21o; note: O, 2, 1, and o denote alcohol oxidation, O2_1, O1_1, and outer-sphere, respectively), and the other is O2_1 → NH_2 → NH_TS1 → NH_1 → O1_1 → O1_2i → O1_TS1i → O1_3i → O2_4i → O2_TS2i → O2_5i → O2_6i → O2_5o (defined as O21i; note: O, 2, 1, and i denote alcohol oxidation, O2_1, O1_1, and inner-sphere, respectively). The apparent activation energies in pathways O2o, O2i, O21o, and O21i are 30.8 (O2_3o relative to O2_1 + $PhCH_2OH$), 31.3, 33.9, and 31.3 kcal mol^{-1}, respectively. Therefore, we can draw the following conclusions: (1) O2o is the most favorable alcohol oxidation pathway, in which the highly apparent activation energy accounts for the high temperature needed to achieve an acceptable reaction rate. (2) O2i and O21i have equal apparent activation energies which are only slightly higher than that in O2o, thus becoming the second favorable alcohol oxidation pathways. (3) Pathway O21o cannot compete with pathways O2o, O2i, and O21i, therefore becoming the most unfavorable alcohol oxidation pathway.

Note that in the above discussion, each of the alcohol oxidation initial steps is an endergonic process. However, the calculations show that all of these processes are downhill in enthalpy (see Table 1). Thus, it is the entropy changes that result in the increase in Gibbs free energy of the alcohol oxidation initial step.

Imine Formation. Aldehyde reacting with primary amine to yield imine and water is a standard organic condensation reaction, and the polar solvent facilitating the imine forming

dx.doi.org/10.1021/cs5004678 | ACS Catal. 2014, 4, 2231−2240

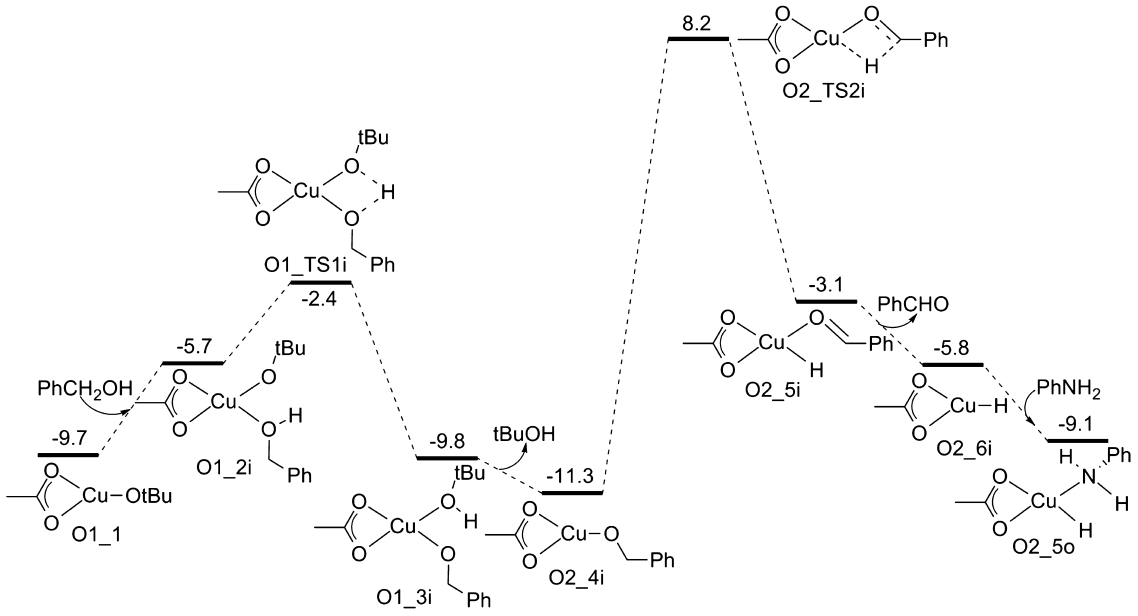

Figure 6. Energy profile for O1_1-catalyzed benzyl alcohol oxidation via the inner-sphere hydrogen transfer pathway. The relative Gibbs free energies are given in kcal mol^{-1}.

Table 1. Changes of Gibbs Free Energy, Enthalpy, and Entropy at the M06//B3LYP and M06//M06 Levels during the Alcohol Oxidation Initial Steps

initial step	ΔG (kcal mol^{-1})	ΔH (kcal mol^{-1})	ΔS (J mol^{-1} K^{-1})
O2_1 + $PhCH_2OH$ → O2_2o	8.2/10.5	−5.4/−6.4	−141.2/−175.5
O2_1 + $PhCH_2OH$ → O2_2i	14.1/13.8	−1.2/−3.2	−158.9/−176.5
O1_1 + $PhCH_2OH$ → O1_2o	5.7/5.5	−10.3/−13.5	−166.2/−197.3
O1_1 + $PhCH_2OH$ → O1_2i	4.0/5.6	−12.5/−14.7	−171.4/−210.8

reaction has been studied theoretically in detail.[29] Thus, We do not model the condensation process (PhCHO + $PhNH_2$ → PhCH═NPh + H_2O) here, but only consider the reaction thermodynamically. The overall imine formation process is endergonic by only 2.9 kcal mol^{-1}. We will directly add this energy to the starting species of imine reduction in the following discussion.

Imine Reduction. Having discussed the alcohol oxidation and the imine formation, we next complete the catalytic cycle by studying the imine reduction. We first consider the outer-sphere hydrogen transfer pathway using the aniline-coordinated copper hydride O2_5o and PhCH═NPh as the beginning reactants (this pathway is defined as R2o; note: R, 2, and o denote imine reduction, O2_5o, and outer-sphere, respectively). As shown in Figure 7, the transition state R2_TS1o for the hydride transfer is located at a free energy of 14.6 kcal mol^{-1} above the beginning reactants. This transition state has a six-membered structure, in which the imine is bound to the aniline ligand by an intramolecular NH···N hydrogen bond of 2.123 Å (see Figure 8), and the hydride is located between the copper and the carbon on the C═N bond (Cu···H = 1.611 Å and C···H = 1.688 Å). The transition state R2_TS1o connects to the H-bonded intermediate R2_1o. This hydride transfer process is moderately exergonic by 8.4 kcal mol^{-1}. The transition state R2_TS2o for the proton transfer is 9.8 kcal mol^{-1} higher than the immediate R2_1o, in which the proton lies midway between the aniline N and the secondary amine N (PhN(H)···H = 1.369 Å and $(PhCH_2)$N···H(Ph) = 1.214 Å),

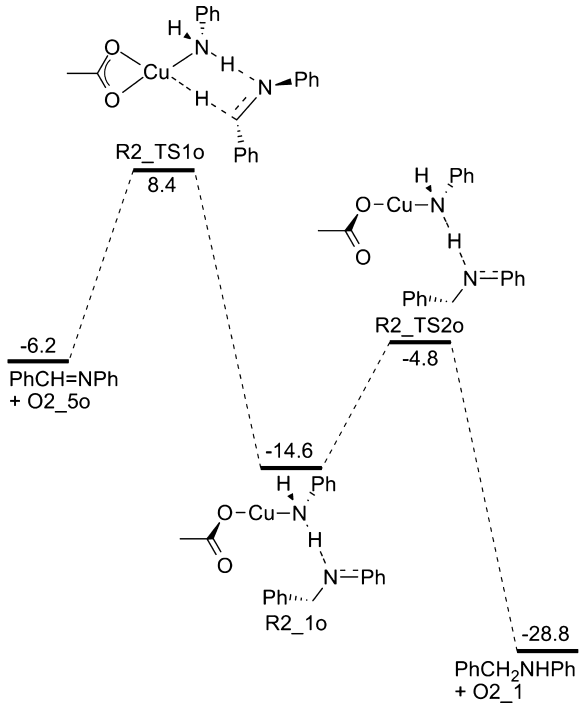

Figure 7. Energy profile for the imine reduction with O2_5o as the reducing intermediate via the outer-sphere hydrogen transfer pathway. The relative Gibbs free energies are given in kcal mol^{-1}.

close to the secondary amine. After the proton transfer, the final second amine product $PhCH_2NHPh$ is obtained, and the active catalyst O2_1 is regenerated.

Next, we consider the inner-sphere hydrogen transfer pathway using the aniline-coordinated copper hydride O2_5o and PhCH═NPh as the beginning reactants. As shown in Figure 9, O2_5o exchanges its $PhNH_2$ ligand with PhCH═NPh to form a slightly stable tetracoordinated intermediate R_1i. This intermediate is well prepared for the hydride transfer from the copper to the imine. The transition state R_TS1i for

dx.doi.org/10.1021/cs5004678 | ACS Catal. 2014, 4, 2231−2240

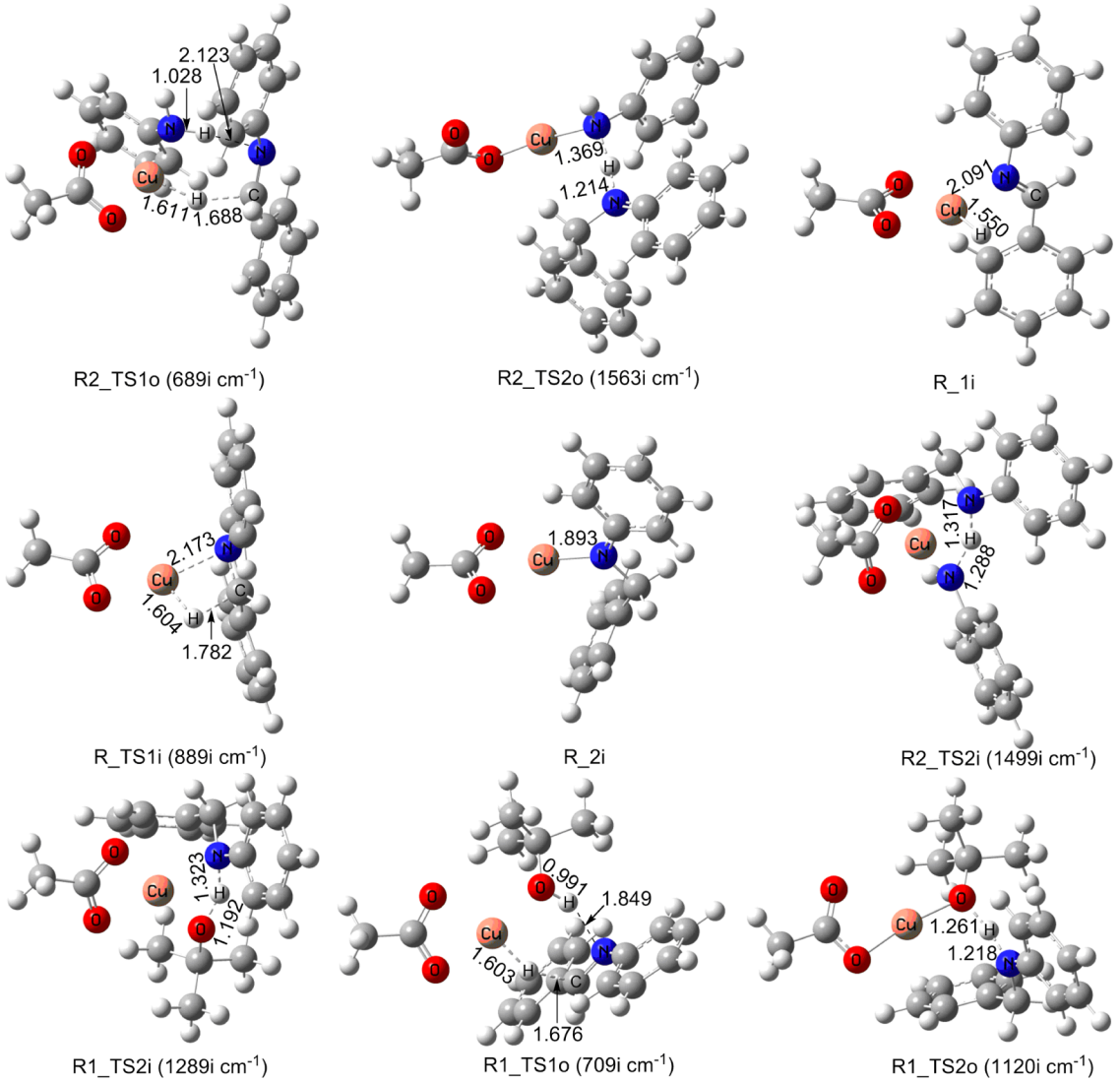

Figure 8. Optimized structures of selected species with selected bond distances (in Å) for the imine reduction. The value in parentheses is the single imaginary frequency that the transition state has.

the hydride transfer is located at a free energy of 17.0 kcal mol^{-1} above R_1i. This transition state has a four-membered structure, in which the distances of Cu···H and C···H are 1.604 and 1.782 Å, respectively (Figure 8). The transition state R_TS1i connects to a very stable tricoordinated Cu(II) complex R_2i (22.5 kcal mol^{-1} below R_1i), which has a short Cu−N bond of 1.893 Å (2.091 Å in R_1i and 2.173 Å in R_TS1i) and a planar Cu center, indicating the formation of a Cu−N π bond.

Protonating the $PhCH_2NPh$ group of R_2i to give the final secondary amine product has two optional pathways: one is using $PhNH_2$ as the proton donor (this pathway together with the hydride transfer (PhCH═NPh + O2_5o → R_2i) is defined as R2i; note: R, 2, and i denote imine reduction, O2_5o, and inner-sphere, respectively); the other is using tBuOH as the proton donor (this pathway together with the hydride transfer (PhCH═NPh + O2_5o → R_2i) and the active catalyst generation (O1_1 + $PhNH_2$ → O2_1 + tBuOH) are defined as R1i; note: R, 1, and i denote imine reduction, O1_3o, and inner-sphere, respectively). As for the proton transfer in R2i, the reaction begins with coordination of $PhNH_2$ to R_2i, leading to the formation of the tetracoordinated complex R2_3i. This step requires a free energy of 12.7 kcal mol^{-1}. The transition state R2_TS2i for the proton transfer is located at a free energy of 15.1 kcal mol^{-1} above R2_3i, in which the distances of PhN(H)···H and $(PhCH_2)$N···H(Ph) are 1.288 and 1.317 Å, respectively. This transition state connects to the $PhCH_2NHPh$-coordinated intermediate R2_4i, which can be easily decomposed into the secondary amine product and the active catalyst O2_1. The proton transfer process in R1i is similar to that in R2i. It can take place by passing the tBuOH-coordinated intermediate R1_3i and the transition state R1_TS2i for the proton transfer. Relative to R_2i + tBuOH, the free energies of R1_3i and R1_TS2i are 14.6 and 24.6 kcal mol^{-1}, respectively. After the proton transfer, the secondary amine product coordinated complex R1_4i can be obtained. Dissociation of the product from R1_4i only requires 1.1 kcal mol^{-1} and gives the complex O1_1, which can react with $PhNH_2$ to regenerate the active catalyst O2_1 via the pathway shown in Figure 1A.

Finally, we consider the imine reduction using O1_3o as the reducing intermediate via the outer-sphere hydrogen transfer pathway (this pathway together with the active catalyst generation (O1_1 + $PhNH_2$ → O2_1 + tBuOH) is defined as R1o; note: R, 1, and o denote imine reduction, O1_3o, and outer-sphere, respectively). As shown in Figure 10, the aniline-coordinated

dx.doi.org/10.1021/cs5004678 | ACS Catal. 2014, 4, 2231−2240

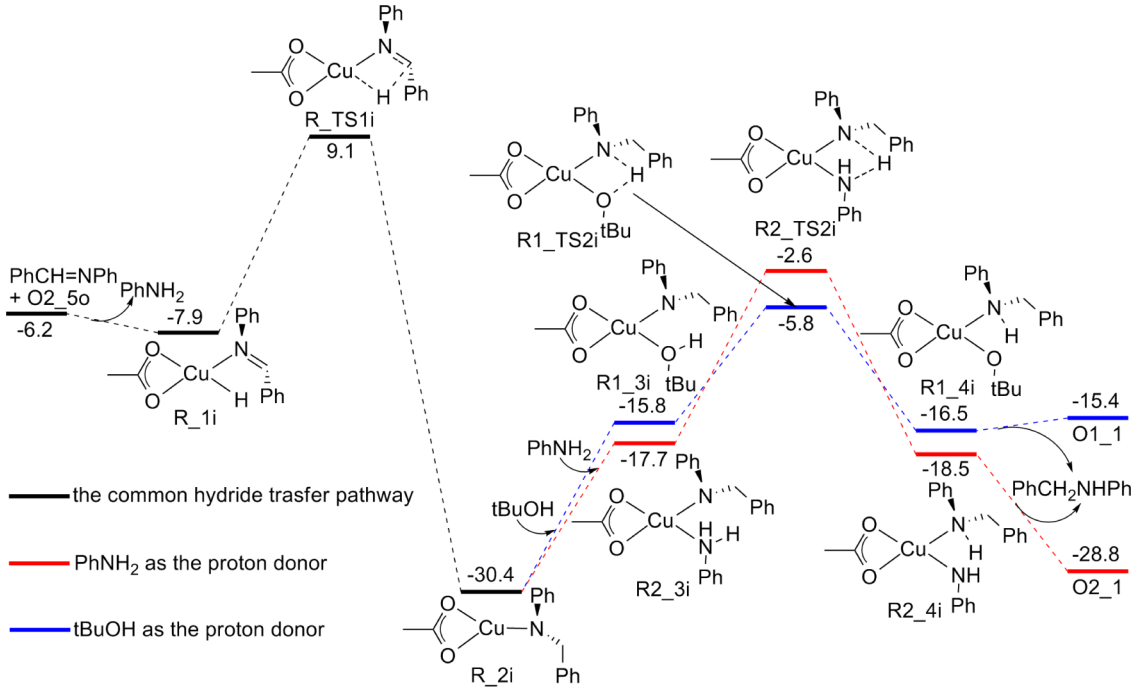

Figure 9. Energy profile for the imine reduction via the inner-sphere hydrogen transfer pathway. The relative Gibbs free energies are given in kcal mol^{-1}.

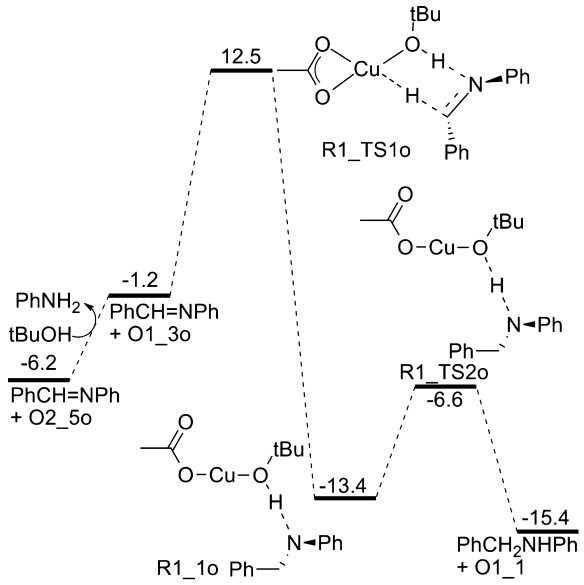

Figure 10. Energy profile for the imine reduction with O1_3o as the reducing intermediate via the outer-sphere hydrogen transfer pathway. The relative Gibbs free energies are given in kcal mol^{-1}.

copper hydride O2_5o and PhCH═NPh are treated as the beginning reactants because O2_5o is more stable than O1_3o. O2_5o can exchange its $PhNH_2$ ligand with tBuOH to give O1_3o by costing a free energy of 5.0 kcal mol^{-1}. Similar to the imine reduction in R2o, this imine reduction from PhCH═NPh + O1_3o to $PhCH_2NHPh$ + O1_1 takes place stepwise by passing the transition states R1_TS1o and R1_TS2o. The six-member transition state R1_TS1o for the hydride transfer, connecting to a stable intermediate R1_1o where the tBuOH ligand is hydrogen bonded to $PhCH_2NPh$ group, is located at a free energy of 13.7 kcal mol^{-1} above PhCH═NPh + O1_3o, while the transition state R1_TS2o for the proton transfer is only 6.8 kcal mol^{-1} higher than the intermediate R1_1o. This transition state leads to the formation of the secondary amine product.

On the basis of the above calculations, we can know that the total reaction Gibbs energies for imine reduction are −22.6, −22.6, −9.2, and −9.2 kcal mol^{-1} in pathways R2o, R2i, R1i, and R1o, respectively, and the apparent activation energies for imine reduction are 14.6, 27.8, 24.6, and 18.7 kcal mol^{-1} in pathways R2o, R2i, R1i, and R1o, respectively. These results indicate that R2o is the most favorable imine reduction pathway.

Discussion with the Energetic Span Model. On the basis of the above discussion, we find O2o−R2o is the most favorable catalytic cycle. To further verify the conclusion and identify the key states influencing the reaction rate, a Fortran program[30] based on the energetic span model[31] is used for TOF and degree of TOF control (X_{TOF}) calculations. The TOF values, X_{TOF}, key state energies, and energetic span values for the proposed reaction pathways are collected in Table 2, from which we can get the following results: (1) O2o−R2o has the highest TOF, 4.0 d^{-1}, verifying that O2o−R2o is the most favorable catalytic cycle. (2) The tricoordinated Cu(II) complex O2_1, the hydride transfer transition state R2_TS1o, and the proton transfer transition state O2_TS1o are the key states influencing the reaction rate, of which the first two are the TDI and the TDTS, respectively. (3) The energetic span between the TDTS and the TDI is 31.5 kcal mol^{-1}. (4) The TOFs in O2i−R2o and O21i−R2o are equal and a little lower than that in O2o−R2o, implying that O2i−R2o and O21i−R2o are the second favorable catalytic cycles. (5) The other pathways are unfavorable because their TOFs are 1 to 2 orders of magnitude smaller than that in O2o−R2o. (6) O2o−R2o, O2i−R2o, and O21i−R2o have equal energetic span values, but their TOFs are not equal, and the main reason for this phenomenon is that the apparent activation energies in the alcohol oxidation processes are different.

dx.doi.org/10.1021/cs5004678 | ACS Catal. 2014, 4, 2231−2240

Table 2. TOF Values (in d^{-1}), Degrees of TOF Control, Key State Energies (in kcal mol^{-1}) at 403.15 K and Energetic Span Values (δE) for the Proposed Reaction Pathways

pathway	TOF	$X_{TOF,I}$	intermediate/ΔG	$X_{TOF,T}$	transition state/ΔG	δE
O2o-R2o	4.0	1.00	O2_1/−23.1	0.65	R2_TS1*o*/8.4	31.5
				0.24	O2_TS1*o*/7.6	
O2o-R2i	0.25	0.88	R_2i/−30.4	0.82	R_TS1*i*/9.1	33.8
O2o-R1i	0.25	0.88	R_2i/−30.4	0.82	R_TS1*i*/9.1	33.8
O2o-R1o	0.036	1.00	O2_1/−23.1	1.00	R1_TS1*o*/12.5	35.6
O2i-R2o	3.5	1.00	O2_1/−23.1	0.56	R2_TS1*o*/8.4	31.5
				0.44	O2_TS2*i*/8.2	
O2i-R2i	0.23	0.88	R_2i/−30.4	0.75	R_TS1*i*/9.1	33.8
O2i-R1i	0.25	0.88	R_2i/−30.4	0.82	R_TS1*i*/9.1	33.8
O2i-R1o	0.036	1.00	O2_1/−23.1	1.00	R1_TS1*o*/12.5	35.6
O21o-R2o	0.29	1.00	O2_1/−23.1	0.95	O1_TS1*o*/10.8	33.9
O21o-R2i	0.033	0.88	R_2i/−30.4	0.89	O1_TS1*o*/10.8	35.5
O21o-R1i	0.033	0.88	R_2i/−30.4	0.89	O1_TS1*o*/10.8	35.5
O21o-R1o	0.033	1.00	O2_1/−23.1	0.89	R1_TS1*o*/12.5	35.6
O21i-R2o	3.5	1.00	O2_1/−23.1	0.56	R2_TS1*o*/8.4	31.5
				0.44	O2_TS2*i*/8.2	
O21i-R2i	0.23	0.88	R_2i/−30.4	0.75	R_TS1*i*/9.1	33.8
O21i-R1i	0.23	0.88	R_2i/−30.4	0.75	R_TS1*i*/9.1	33.8
O21i-R1o	0.036	1.00	O2_1/−23.1	1.00	R1_TS1*o*/12.5	35.6

Table 3. Key State Energies (in kcal mol^{-1}) at Different DFT Levels and TOF Values (in d^{-1})

key state	M06//B3LYP	M06//BLYP	M06//TPSSTPSS	M06//M06
O2_1	−23.1	−26.8	−23.9	−26.0
O2_TS1o	7.6	4.3	6.8	6.0
O2_3o	7.7	4.4	7.3	6.5
O2_TS2o	7.0	2.7	5.2	4.4
O2_5o	−9.1	−12.7	−10.8	−10.7
R2_TS1o	8.4	4.9	7.2	8.3
TOF in O2o-R2o	4.0	3.1	6.0	0.17
O2_TS2i	8.2	5.4	7.9	6.8
TOF in O2i/O21i-R2o[a]	3.5	1.6	2.9	0.16

[a]O2i-R2o and O21i-R2o have the common key states and TOFs.

To test the functional dependence, we recalculated the key state energies selected on the basis of the energetic span model. The energetic results are shown in Table 3. These additional calculations further support that alcohol oxidation takes place in a stepwise manner via the outer-sphere hydrogen transfer pathway, and O2o−R2o is the most favorable catalytic cycle.

CONCLUSIONS

DFT calculations have been performed to study the mechanism of $Cu(AcO)_2$/tBuOK-catalyzed N-alkylation of amino derivatives with primary alcohols by choosing $PhNH_2$ and $PhCH_2OH$ as the reagents. A viable catalytic cycle, involving the mechanism postulated by Martínez-Asencio et al.,[11,12] has been found, which contains three sequential steps: alcohol oxidation, imine formation, and imine reduction. For alcohol oxidation, the outer-sphere hydrogen transfer is the most favorable pathway, in which the two hydrogen atoms successively eliminated from benzyl alcohol in the form of the proton and the hydride are respectively transferred to the $PhNH^-$ ligand and the metal of the active catalyst O2_1 to generate the aniline-coordinated Cu hydride O2_5o and benzaldehyde (Figure 2). For imine reduction, the aniline-coordinated Cu hydride O2_5o is the reducing intermediate and the outer-sphere hydrogen transfer is also the most favorable pathway, in which the hydride and the proton on complex O2_5o are separately added to carbon and nitrogen on the C=N bond of the imine to give the secondary amine product and regenerate the active catalyst O2_1 in a stepwise manner (Figure 7). The calculated TOF roughly agrees with the experimental observation and, therefore, further supports the validity of the proposed hydrogen transfer mechanism. This theoretical study can provide important insights for understanding N-alkylation of amino derivatives with primary alcohols catalyzed by other transition metal complexes.

ASSOCIATED CONTENT

Supporting Information

Detailed optimized geometries, energies, and thermal corrections to Gibbs free energies. This material is available free of charge via the Internet at http://pubs.acs.org/.

AUTHOR INFORMATION

Corresponding Authors

*E-mail: huiling@jlu.edu.cn.
*E-mail: huangxr@jlu.edu.cn.

Notes

The authors declare no competing financial interest.

ACKNOWLEDGMENTS

The authors thank the National Basic Research Program of China (973 Program; 2012CB932800f), the National Natural Science Foundation of China (No. 21073075), and the National Natural Science Foundation of China (No. 21303067) for financial support of this research.

REFERENCES

(1) (a) Severin, R.; Doye, S. *Chem. Soc. Rev.* **2007**, *36*, 1407−1420. (b) Doye, S. *Synlett* **2004**, *10*, 1653−1672. (c) Inaf, S. S.; Witiak, D. T. *Synthesis* **1999**, *3*, 435−440. (d) Müller, T.; Beller, M. *Chem. Rev.* **1998**, *98*, 675−704. (e) Hultzsch, K. C. *Adv. Synth. Catal.* **2005**, *347*, 367−391.

(2) (a) Hartwig, J. F. *Synlett* **2006**, *9*, 1283−1294. (b) Navarro, O.; Marion, N.; Mei, J.; Nolan, S. P. *Chem.—Eur. J.* **2006**, *12*, 5142−5148. (c) Li, X.; Mintz, E. A.; Bu, X. R.; Zehnder, O.; Bosshard, C.; Gunter, P. *Tetrahedron* **2000**, *56*, 5785−5791. (d) Wolfe, J. P.; Buchwald, S. L. *J. Am. Chem. Soc.* **1997**, *119*, 6054−6058.

(3) (a) Bhattacharyya, S. J. *Org. Chem.* **1995**, *60*, 4928−4929. (b) Abdel-Magid, A. F.; Carson, K. G.; Harris, B. D.; Maryan-off, C. A.; Shah, R. D. *J. Org. Chem.* **1996**, *61*, 3849−3862. (c) Mizuta, T.; Sakagushi, S.; Ishii, Y. *J. Org. Chem.* **2005**, *70*, 2195−2199.

(4) (a) Hamid, M. H. S. A.; Slatford, P. A.; Williams, J. M. J. *Adv. Synth. Catal.* **2007**, *349*, 1555−1575. (b) Dobereiner, G. E.; Grabtree, R. H. *Chem. Rev.* **2010**, *110*, 681−703. (c) Guillena, G.; Ramon, D.; Yus, M. *Chem. Rev.* **2010**, *110*, 1611−1641. (d) Nixon, T. D.; Whittlesey, M. K.; Williams, J. M. J. *Dalton Trans.* **2009**, *5*, 753−762.

(5) (a) Watanabe, Y.; Morisaki, Y.; Kondo, T.; Mitsudo, T. *J. Org. Chem.* **1996**, *61*, 4214−4218. (b) Watanabe, Y.; Tsuji, Y.; Ohsugi, Y. *Tetrahedron Lett.* **1981**, *22*, 2667−2670. (c) Tillack, A.; Hollmann, D.; Michalik, D.; Beller, M. *Tetrahedron Lett.* **2006**, *47*, 8881−8885. (d) Hollmann, D.; Tillack, A.; Michalik, D.; Jackstell, R.; Beller, M. *Chem.—Asian J.* **2007**, *2*, 403−410.

(6) Tsuji, Y.; Takeuchi, R.; Ogawa, H.; Watanabe, Y. *Chem. Lett.* **1986**, *3*, 293−294.

(7) Tanaka, N.; Hatanka, M.; Watanabe, Y. *Chem. Lett.* **1992**, *21*, 575−578.

(8) (a) Cami-Kobeci, G.; Williams, J. M. J. *Chem. Commun.* **2004**, *9*, 1072−1073. (b) Cami-Kobeci, G.; Slatford, P. A.; Whittlesey, M. K.; Williams, J. M. J. *Bioorg. Med. Chem. Lett.* **2005**, *15*, 535−537.

(c) Yamaguchi, R.; Kawagoe, S.; Asai, C.; Fujita, K. I. *Org. Lett.* **2008**, *10*, 181−184.
(9) Shi, F.; Tse, M. K.; Cui, X.; Gördes, D.; Michalik, D.; Thurow, K.; Deng, Y.; Beller, M. *Angew. Chem., Int. Ed.* **2009**, *48*, 5912−5915.
(10) Cui, X.; Shi, F.; Tse, M. K.; Gördes, D.; Thurow, K.; Beller, M.; Deng, Y. *Adv. Synth. Catal.* **2009**, *351*, 2949−2958.
(11) Martínez-Asencio, A.; Ramón, D. J.; Yus, M. *Tetrahedron Lett.* **2010**, *51*, 325−327.
(12) Martínez-Asencio, A.; Ramón, D. J.; Yus, M. *Tetrahedron* **2011**, *67*, 3140−3149.
(13) (a) Bosson, J.; Poater, A.; Cavallo, L.; Nolan, S. P. *J. Am. Chem. Soc.* **2010**, *132*, 13146−13149. (b) Nova, A.; Balcells, D.; Schley, N. D.; Dobereiner, G. E.; Crabtree, R. H.; Eisenstein, O. *Organometallics* **2010**, *29*, 6548−6558. (c) Sieffert, N.; Bühl, M. *J. Am. Chem. Soc.* **2010**, *132*, 8056−8070. (d) Comas-Vives, A.; Ujaque, G.; Lledós, A. *Organometallics* **2007**, *26*, 4135−4144. (e) Handgraaf, J.-W.; Meijer, E. J. *J. Am. Chem. Soc.* **2007**, *129*, 3099−3103. (f) Privalov, T.; Samec, J. S. M.; Bäckvall, J.-E. *Organometallics* **2007**, *26*, 2840−2848. (g) Yamakawa, M.; Ito, H.; Noyori, R. *J. Am. Chem. Soc.* **2000**, *122*, 1466−1478. (h) Balcells, D.; Nova, A.; Clot, E.; Gnanamgari, D.; Crabtree, R. H.; Eisenstein, O. *Organometallics* **2008**, *27*, 2529−2535. (i) Fristrup, P.; Tursky, M.; Madsen, R. *Org. Biomol. Chem.* **2012**, *10*, 2569−2577.
(14) Becke, A. D. *J. Chem. Phys.* **1993**, *98*, 5648−5652.
(15) Lee, C.; Yang, W.; Parr, R. G. *Phys. Rev. B* **1988**, *37*, 785−789.
(16) Marenich, A. V.; Cramer, C. J.; Truhlar, D. G. *J. Phys. Chem. B* **2009**, *113*, 6378−6396.
(17) Krishnan, R.; Binkley, J. S.; Seeger, R.; Pople, J. A. *J. Chem. Phys.* **1980**, *72*, 650−654.
(18) Hay, P. J.; Wadt, W. R. *J. Chem. Phys.* **1985**, *82*, 299−310.
(19) Hehre, W. J.; Ditchfield, R.; Pople, J. A. *J. Chem. Phys.* **1972**, *56*, 2257−2261.
(20) (a) Zhang, S. L.; Liu, L.; Fu, Y.; Guo, Q. X. *Organometallics* **2007**, *26*, 4546−4554. (b) Yoshikai, N.; Zhang, S. L.; Nakamura, E. *J. Am. Chem. Soc.* **2008**, *130*, 12862−12863. (c) Poater, A.; Ribas, X.; Llobet, A.; Cavallo, L.; Solà, M. *J. Am. Chem. Soc.* **2008**, *130*, 17710−17717. (d) Yu, H. Z.; Jiang, Y. Y.; Fu, Y.; Liu, L. *J. Am. Chem. Soc.* **2010**, *132*, 18078−18091 and references cited therein.
(21) (a) Fukui, K. *J. Phys. Chem.* **1970**, *74*, 4161−4163. (b) Fukui, K. *Acc. Chem. Res.* **1981**, *14*, 363−368.
(22) (a) Zhao, Y.; Truhlar, D. G. *J. Chem. Phys.* **2006**, *125*, 194101−194118. (b) Zhao, Y.; Truhlar, D. G. *Acc. Chem. Res.* **2008**, *41*, 157−167.
(23) (a) Roy, L. E.; Hay, P. J.; Martin, R. L. *J. Chem. Theory Comput.* **2008**, *4*, 1029−1031. (b) Ehlers, A. W.; Bohme, M.; Dapprich, S.; Gobbi, A.; Hollwarth, A.; Jonas, V.; Kohler, K. F.; Stegmann, R.; Veldkamp, A.; Frenking, G. *Chem. Phys. Lett.* **1993**, *208*, 111−114.
(24) Becke, A. D. *Phys. Rev. A* **1988**, *38*, 3098−3100.
(25) Tao, J. M.; Perdew, J. P.; Staroverov, V. N.; Scuseria, G. E. *Phys. Rev. Lett.* **2003**, *91*, 146401−146404.
(26) Frisch, M. J.; Trucks, G. W.; Schlegel, H. B.; Scuseria, G. E.; Robb, M. A.; Cheeseman, J. R.; Scalmani, G.; Barone, V.; Mennucci, B.; Petersson, G. A.; Nakatsuji, H.; Caricato, M.; Li, X.; Hratchian, H. P.; Izmaylov, A. F.; Bloino, J.; Zheng, G.; Sonnenberg, J. L.; Hada, M.; Ehara, M.; Toyota, K.; Fukuda, R.; Hasegawa, J.; Ishida, M.; Nakajima, T.; Honda, Y.; Kitao, O.; Nakai, H.; Vreven, T.; Montgomery, J. A., Jr.; Peralta, J. E.; Ogliaro, F.; Bearpark, M.; Heyd, J. J.; Brothers, E.; Kudin, K. N.; Staroverov, V. N.; Kobayashi, R.; Normand, J.; Raghavachari, K.; Rendell, A.; Burant, J. C.; Iyengar, S. S.; Tomasi, J.; Cossi, M.; Rega, N.; Millam, N. J.; Klene, M.; Knox, J. E.; Cross, J. B.; Bakken, V.; Adamo, C.; Jaramillo, J.; Gomperts, R.; Stratmann, R. E.; Yazyev, O.; Austin, A. J.; Cammi, R.; Pomelli, C.; Ochterski, J. W.; Martin, R. L.; Morokuma, K.; Zakrzewski, V. G.; Voth, G. A.; Salvador, P.; Dannenberg, J. J.; Dapprich, S.; Daniels, A. D.; Farkas, Ö.; Foresman, J. B.; Ortiz, J. V.; Cioslowski, J.; Fox, D. J. *Gaussian 09*, revision A.02; Gaussian, Inc.: Wallingford, CT, 2009.
(27) Li, H. X.; Jiang, J. L.; Lu, G.; Huang, F.; Wang, Z. X. *Organometallics* **2011**, *30*, 3131−3141.
(28) Zhao, L. L.; Li, H. X.; Lu, G.; Wang, Z. X. *Dalton Trans.* **2010**, *39*, 4038−4047.
(29) Hall, N. E.; Smith, B. J. *J. Phys. Chem. A* **1998**, *102*, 4930−4938.
(30) Carvajal, M. A.; Kozuch, S.; Shaik, S. *Organometallics* **2009**, *28*, 3656−3665.
(31) (a) Amatore, C.; Jutand, A. *J. Organomet. Chem.* **1999**, *576*, 254−278. (b) Kozuch, S.; Shaik, S. *J. Am. Chem. Soc.* **2006**, *128*, 3355−3365. (c) Kozuch, S.; Shaik, S. *J. Phys. Chem. A* **2008**, *112*, 6032−6041. (d) Kozuch, S.; Shaik, S. *Acc. Chem. Res.* **2010**, *44*, 101−110.